Hindawi Publishing Corporation
Journal of Nanomaterials
Volume 2015, Article ID 195024, 9 pages
http://dx.doi.org/10.1155/2015/195024

Research Article

Preparation of High Activity Ga and Cu Doped ZnS by Hydrothermal Method for Hydrogen Production under Visible Light Irradiation

Melody Kimi,[1,2] Leny Yuliati,[3] and Mustaffa Shamsuddin[1]

[1]*Department of Chemistry, Faculty of Science, Universiti Teknologi Malaysia, 81310 Johor Bahru, Johor, Malaysia*
[2]*Centre for Pre-University Studies, Universiti Malaysia Sarawak, 94300 Kota Samarahan, Sarawak, Malaysia*
[3]*Ibnu Sina Institute for Fundamental Science Studies, Universiti Teknologi Malaysia, 81310 Johor Bahru, Johor, Malaysia*

Correspondence should be addressed to Melody Kimi; kmelody@preuni.unimas.my

Received 6 May 2015; Accepted 14 July 2015

Academic Editor: Balachandran Jeyadevan

Ga(0.1),Cu(x)-ZnS (x = 0.01, 0.03, 0.05) photocatalysts were successfully synthesized by hydrothermal method. The synthesized Ga and Cu codoped ZnS photocatalysts showed photocatalytic property effective for hydrogen production from aqueous solution containing Na_2SO_3 and Na_2S as sacrificial reagent under visible light irradiation. The rate of hydrogen production was found to be strongly dependent on Cu doping content. The highest photocatalytic activity is observed for Ga(0.1),Cu(0.01)-ZnS with hydrogen production rate of 114 μmol/h. The addition of Ga as codoped increased the photocatalytic activity to 58 times as compared to single doped Cu-ZnS. The Ga and Cu codoped ZnS photocatalysts are also stable under long irradiation. The enhancement in the photocatalytic activity of Ga and Cu codoped photocatalyst can be attributed to the synergistic effect between Ga and Cu. The photocatalytic activity was greatly enhanced with the addition of 0.5 wt% Ru as cocatalyst with a hydrogen production rate of 744 μmol/h.

1. Introduction

Hydrogen, an attractive clean energy source with high energy capacity, is a very promising candidate as a primary energy source in the future [1, 2]. Photocatalytic water splitting is considered as an alternative method to produce hydrogen utilizing solar energy. Up to now, considerable efforts have been devoted to developing highly active photocatalysts for the water splitting reaction and remarkable progress has been made [3–6].

ZnS is known to be a highly active photocatalyst for hydrogen evolution from aqueous solutions containing sacrificial reagents such as SO_3^{2-} and S^{2-}, even without the addition of Pt cocatalyst. This is due to the high conduction band level of ZnS to reduce water to hydrogen [7–9]. However, the large band gap of ZnS restricts its photocatalytic applications within the UV light range. To effectively utilize solar light energy, visible light response photocatalysts with high photocatalytic activity are desired.

Doping of ZnS is considered as one of the many ways to enhance the light absorption ability of ZnS to the visible light region while still maintaining the high conduction band. Cu doped ZnS [10, 11], Ni doped ZnS [12], and Bi doped ZnS [13] have been reported to show considerable high photocatalytic activities for hydrogen evolution under visible light from aqueous solution containing S^{2-} and/or SO_3^{2-} as electron donors. The visible light response is obtained by the formation of donor levels by the doped metal cations in the wide band gap of the ZnS host material.

Although Cu doped ZnS [10] showed high photocatalytic activity for hydrogen evolution, it suffers from photocorrosion. One of the possible methods to maintain the high photocatalytic activity of Cu doped ZnS without suffering from photocorrosion is to carry out doping with another metal. It is known that codoping is effective to suppress the recombination rate of electron-hole pairs [14, 15]. This is due to the synergic effects produced when two metals are doped together. The negative effects caused by doping

can be partially improved by codoping with another dopant. Dopants like Sn^{4+} and Eu^{3+} were incorporated in TiO_2 to improve the visible light absorption and photocatalytic activity. The purpose of using Sn and Eu was that the former is known to help in the charge separation of photogenerated electrons and holes and the latter being a lower valent cation than Ti^{4+} can generate anion vacancies in TiO_2 thereby leading to visible light absorption [14].

Ga doped ZnS has been reported to be photocatalytically active under UV light irradiation [16]. In addition to the absorption spectrum, the mobility of photogenerated charges is critical for photocatalytic activity. Metal compounds associated with d^{10} electronic configurations such as Ga^{3+} are attractive because their conduction and valence bands are formed by hybridized sp orbitals with large band dispersion that would lead to high charge mobility and, hence, high photocatalytic performance [17, 18]. Ga was selected as the dopant in this study as it is regarded as the most efficient donor for ZnS to generate more charge carriers [19].

This present study aims to investigate the exact role of synergistic effect of codoping Ga and Cu into ZnS lattice in the physical-chemical properties and photocatalytic activity for hydrogen production. The new photocatalyst Ga, Cu codoped ZnS was prepared by using hydrothermal method. The role of Ga in promoting the photocatalytic activity was also examined.

2. Experimental

2.1. Synthesis of Samples. Simple hydrothermal method was used to synthesize the powder samples of ZnS, Cu(0.1)-ZnS, Ga(0.1)-ZnS, and Ga(0.1),Cu(x)-ZnS ($x = 0.01, 0.03, 0.05$) in a similar way to the previous literatures [20, 21]. The samples were labelled as Ga(0.1),Cu(x)-ZnS, with x showing the doping amount of Cu in mol ratio. In a typical synthesis for Ga(0.1),Cu(0.01)-ZnS, 0.2 mmol of $Cu(NO_3)_2{\cdot}3H_2O$ (Fluka, 98%), 2 mmol of $Ga(NO_3)_2{\cdot}xH_2O$ (Aldrich, 99.9%), 18 mmol of $Zn(CH_3COO)_2{\cdot}2H_2O$ (GCE chemicals, 98%), and 20 mmol of CH_3CSNH_2 (Merck, 99%) were dissolved in 50 mL of distilled water. The solution was added to an autoclave that was sealed and heated in an oven at 433 K for 8 h. After natural cooling to room temperature, the precipitates were washed with distilled water for several times and dried in vacuum at room temperature.

2.2. Characterization. Powder X-ray diffraction (XRD) patterns were obtained with an X-ray diffractometer, Bruker Advance D8 Siemens 5000 using Cu Kα radiation (λ = 0.15418 nm, 40 kV, 40 mA). The diffuse reflectance UV-visible (DR UV-vis) spectra were recorded on a Perkin Elmer Ultraviolet-Visible Spectrometer Lambda 900. Barium sulfate ($BaSO_4$) was used as the reference. Photoluminescence (PL) spectra were measured at room temperature using a photoluminescence spectrophotometer (PTI QM-4) with an excitation wavelength of 250 nm. The morphologies and crystal sizes of the samples were determined with field emission scanning electron microscopy (FESEM) using JEOL JSM 6701F with platinum coating (2 kV, 10 mA). Specific surface area was measured using the Brunauer-Emmett-Teller (BET) method, Beckman Coulter SA3100 by nitrogen absorption at 77 K. The samples were previously outgassed at 393 K for 180 min. The elemental analysis was completed on a Bruker S4 PIONEER X-ray fluorescence (XRF) spectrum, using Ru target and 4 kW power.

The chemical forms of the products were studied using X-ray photoelectron spectroscopy (XPS), AXIS Ultra DLD, Shimadzu, with monochromatic Al Kα radiation (1486.6 eV).

2.3. Photocatalytic Activities. Photocatalytic hydrogen evolution was performed in a closed-side irradiated-Pyrex cell equipped with an outer water cooling system to keep the temperature throughout the reaction at 25 ± 0.2°C. In all experiments, the powder sample (0.2 g) was dispersed by magnetic stirring in an aqueous solution (190 mL) containing 0.25 M Na_2SO_3 and 0.35 M Na_2S [20] as sacrificial agents. Nitrogen gas was purged through the reaction cell for 30 min before reaction to remove air. A 300 W Xe lamp was focused on the side window of the cell through a cut-off filter ($\lambda \geq$ 425 nm, TrusTech PLS-SXE 300). The apparent quantum yields (AQY) defined by (1) were measured using a 425 nm band pass filter and Avantes fibre optic spectrometer (Ava Spec USB 2000) connected to AveSoft 7.2. The amount of hydrogen evolved was determined with a thermal conductivity detector (TCD) gas chromatography (SP 2100) using NaX zeolite column and nitrogen as carrier gas. Cocatalyst ruthenium (0.1–1 wt%) was loaded on the photocatalyst surface by an *in situ* photodeposition method from the precursor of $RuCl_3$. Consider

$$\begin{aligned} \text{AQY}\,(\%) &= \frac{\text{number of reacted electrons}}{\text{number of incident photons}} \times 100 \\ &= \frac{\text{number of evolved } H_2 \text{ molecules}}{\text{number of incident photons}} \times 2. \end{aligned} \tag{1}$$

3. Results and Discussion

3.1. Crystal Structure. Figure 1 shows XRD patterns of ZnS, Cu(0.1)-ZnS, Ga(0.1)-ZnS, and Ga(0.1),Cu(x)-ZnS powder samples. The distinctive peaks are found at 2θ of 28.6, 32.5, 47.6, and 56.3, corresponding to the (111), (200), (220), and (311) planes, respectively, which is a typical pattern of cubic zinc blende phase [22, 23]. For ZnS, there is shoulder peak at $2\theta = 27$. This is due to (100) and (002) plane hexagonal phase of ZnS, which is in agreement with the reported values with similar synthesis temperature [24]. As for the Cu(0.1)-ZnS sample, there is a broad shoulder peak at $2\theta = 27$ which might be due to the (101) plane of CuS [25]. This peak has a different shape compared to the shoulder peak of ZnS at the same place. Furthermore, the peak at $2\theta = 30.5$ also disappeared for Cu(0.1)-ZnS. It is also observed that there is a shoulder peak at $2\theta = 33.5$ and $2\theta = 59$ corresponding to (006) and (116) plane of CuS, respectively [26, 27]. This confirms that, for Cu(0.1)-ZnS, both CuS and ZnS phases existed in the sample.

The peak became broad with the addition of Ga to the samples; thus the weak diffraction peak at (200) was not

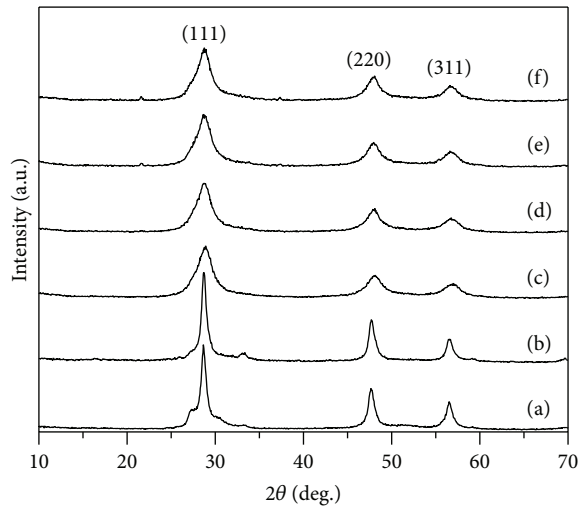

FIGURE 1: XRD patterns of (a) ZnS, (b) Cu(0.1)-ZnS, (c) Ga(0.1)-ZnS, (d) Ga(0.1),Cu(0.01)-ZnS, (e) Ga(0.1),Cu(0.03)-ZnS, and (f) Ga(0.1),Cu(0.05)-ZnS.

observed. Ga(0.1),Cu(x)-ZnS samples showed well developed cubic zinc blende phase without any impurity phase or elements. No peaks corresponding to metallic Ga or Cu or oxides were observed in the XRD pattern because of the low dopant concentration. This could also be due to the highly dispersed Ga and Cu in or on the ZnS particle.

The diffraction peaks of ZnS were intense, suggesting a well crystallized sample. For Cu(0.1)-ZnS, the peak intensity increased and became sharper, indicating an increase in crystallinity. This suggests that Cu promotes the crystal growth due to crystal metallization effect [28]. In contrast, for Ga(0.1)-ZnS and Ga(0.1),Cu(x)-ZnS samples, they showed broad and weak diffraction peaks. This is probably due to the the low crystallinity caused by defect sites or the addition of Ga inhibited crystal growth. However, as the amount of Cu dopant increased from 0.01 to 0.05 mol, there were no changes in peak intensities. This indicates that the amount of Cu did not have any effect on the crystal structure.

There was no peak shifting from ZnS when only Cu was doped into ZnS due to similar ionic radii of Cu^{2+} (0.72 Å) and Zn^{2+} (0.74 Å). However, for Ga(0.1)-ZnS and Ga(0.1),Cu(x)-ZnS samples, there was slight shifting of peak to higher angle. This might be due to the smaller ionic radius of Ga^{3+} (0.62 Å) compared to Zn^{2+} which means Ga ions easily enter the lattice of ZnS without causing distortion.

The crystallite size of the prepared samples is calculated from the (111) diffraction peak using Scherrer equation as shown in Table 1. From Table 1, it was revealed that, in the presence of Cu in ZnS, the crystallite size increased which is confirmed from the increase in peak intensity. The decrease in crystallite size can be observed for all Ga doped ZnS samples, which suggests that Ga inhibits the growth of crystal. The slight increase of crystallite size when the amount of Cu was increased in the Ga(0.1),Cu(x)-ZnS samples could be attributed to the larger ionic radius of Cu from Ga. From Table 1, the slight changes in d-spacing and lattice parameter for all the Ga(0.1),Cu(x)-ZnS from ZnS indicated that some substitution of Zn^{2+} ions by the doping metal ions had taken place. For Cu(0.1)-ZnS, the lattice parameter decreased compared to ZnS; this may be caused by the substitution of Zn^{2+} (0.74 Å) by Cu^{2+} (0.72 Å). The same pattern was observed with Ga(0.1)-ZnS. For Ga(0.1),Cu(x)-ZnS, the lattice parameter remained unchanged regardless of the Cu amount, indicating that no further substitution has taken place above Cu content of 0.01.

3.2. Morphology. The FESEM images of ZnS, Cu(0.1)-ZnS, Ga(0.1)-ZnS, and Ga(0.1),Cu(x)-ZnS are shown in Figure 2. The particles size of ZnS and Cu(0.1)-ZnS ranges from 20 to 150 nm. The nanospheres agglomerated into a bigger undefined shape. As Ga was doped into ZnS, the smaller nanospheres in the range of 10 nm to 50 nm compacted and agglomerated into bigger spheres in the range of 1 μm. The substitution of Zn by Ga ions might cause the formation of defects due to different ionic radius. The increase in defect sites inhibits the growth of crystal. The smaller nanospheres observed which are formed by the addition of Ga were confirmed by the weak and broad intensities of XRD peaks. The smaller size of nanospheres with the addition of Ga can be ascribed to the Ga localizing near the surface of crystal which prevented crystal growth. Ga(0.1),Cu(x)-ZnS have smaller single sphere that makes it easier to agglomerate into bigger spheres compared to ZnS. It can be deduced that the addition of Ga led to the formation of sphere shaped particles.

From the BET analysis in Table 1, ZnS had a surface area of 57 m^2/g. For Cu(0.1)-ZnS, as the particle size becomes larger due to the presence of Cu, the surface area decreases to 38 m^2/g. The addition of Ga dopant increased the specific surface area for Ga(0.1)-ZnS and Ga(0.1),Cu(0.01)-ZnS. This is in good agreement with the XRD and FESEM results. On the other hand, decrease in specific surface area is observed when the samples had higher amount of Cu dopant. It can be suggested that the excess Cu on the catalyst surface led to the decrease in surface area.

3.3. Optical Properties

3.3.1. Diffuse Reflectance UV-Visible Spectra. The absorption spectra of investigated samples are shown in Figure 3. The onset of the absorption edge of ZnS is at 400 nm in the UV absorption region, corresponding to the band gap of 3.25 eV, which is slightly lower than the value usually reported (3.6–3.7 eV) [29, 30]. This might be due to the synthesis procedure which resulted in defects that might decrease the band gap energy [11]. It can be seen from Figure 3(b) that extended absorption is generated in the visible light region when Cu is doped. A large absorption shoulder at 550 nm to 800 nm was observed for Cu(0.1)-ZnS which may be due to Cu d-d transition in a large amount. The shoulder peak around 400 nm [31] and around 650 nm [25] shows the existence of CuS phase in the Cu(0.1)-ZnS as confirmed by XRD. As for Ga(0.1)-ZnS, only a slight shift to longer wavelength from ZnS but not to the visible light region was observed. This could be deduced from the formation of defects from the doping of Ga into the Zn lattices.

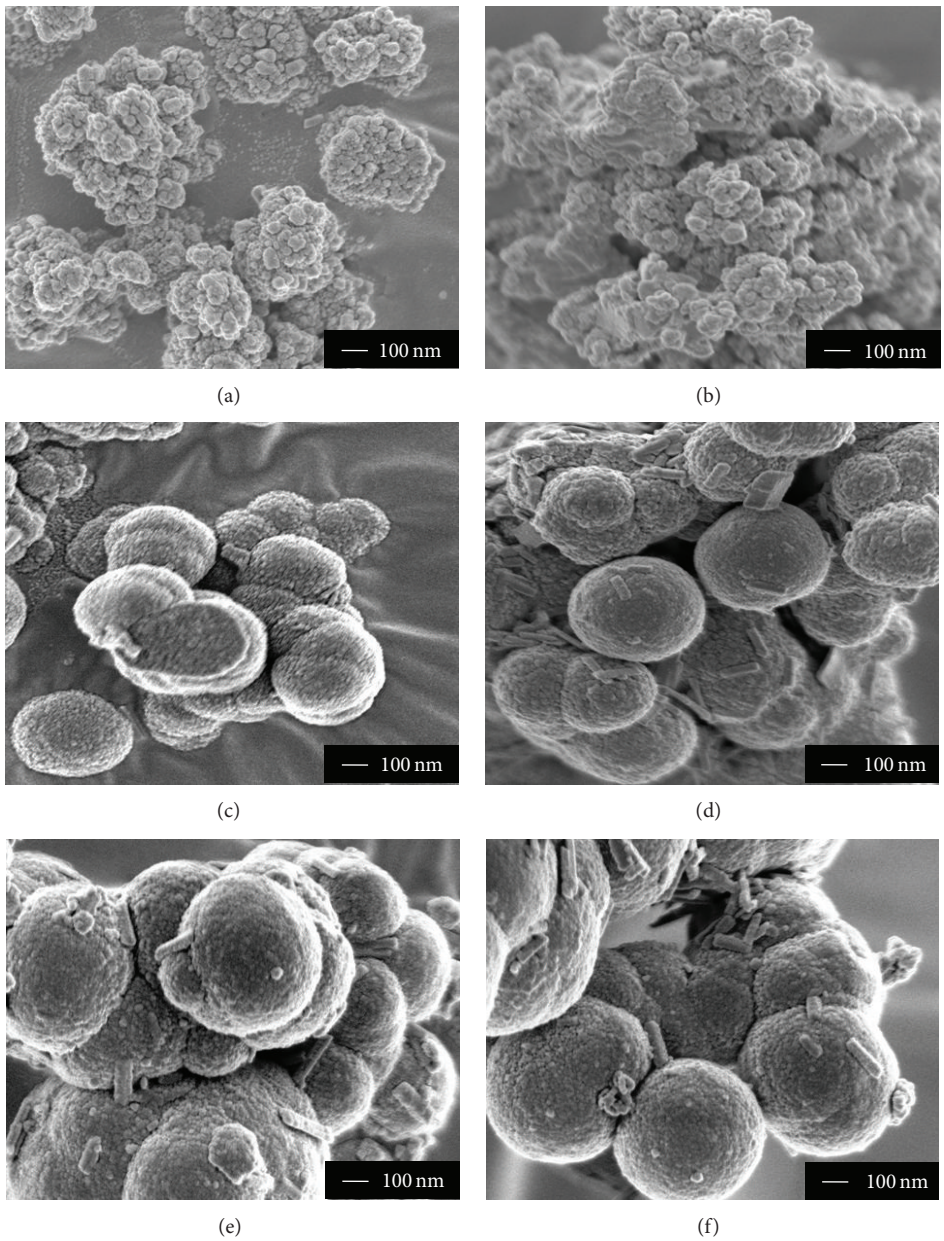

Figure 2: FESEM images of (a) ZnS, (b) Cu(0.1)-ZnS, (c) Ga(0.1)-ZnS, (d) Ga(0.1),Cu(0.01)-ZnS, (e) Ga(0.1),Cu(0.03)-ZnS, and (f) Ga(0.1),Cu(0.05)-ZnS.

As for Ga(0.1),Cu(x)-ZnS samples, with increasing amount of Cu dopant, the absorption edges gradually shifted to longer wavelength. The absorption edge of Ga(0.1),Cu(x)-ZnS is located between that of ZnS and that of Cu(0.1)-ZnS and shifts monotonously from 490 nm to 550 nm with an increase in x from 0.01 to 0.05. As the amount of Cu increased, the intensity of the absorption tail at 550 nm to 800 nm also increased due to the Cu d-d transition of Cu^{2+} [10, 11, 32, 33]. This suggests that more Cu is present on the surface of the samples. The extension of the absorption edge to the visible region and increasing absorption tail implied that Cu was incorporated not only into the lattice of ZnS but also on the surface.

Comparing the spectra of Ga(0.1)-ZnS and Cu(0.1)-ZnS, it can be concluded that the visible light response of Ga(0.1),Cu(x)-ZnS is derived from the doping of Cu instead of Ga. It can be deduced that the absorption edge around 500 nm was due to the charge transfer from Cu^{2+} 3d orbital to Zn 4s4p orbital. The absorption tail observed above 550 nm could be ascribed to d-d transition of Cu in the Ga(0.1),Cu(x)-ZnS samples. The doped Cu forms a new energy level in the band structure of Ga(0.1)-ZnS. The charge transfer from donor levels formed by Cu 3d to the conduction band leads to the visible light response.

The band gap energies of the samples were estimated from Tauc's plots as seen in Table 1. The valence band of

Table 1: Properties of ZnS and ZnS doped samples.

Entry	Samples	d_{111} value[a] (Å)	Lattice parameter, a[b] (nm)	Crystallite size, d[c] (nm)	Band gap (eV)[d]	Surface area (m^2/g)
1	ZnS	3.1121	5.3903	11.76	3.25	57
2	Cu(0.1)-ZnS	3.1068	5.3811	12.51	1.75	39
3	Ga(0.1)-ZnS	3.0857	5.3447	4.48	3.02	113
4	Ga(0.1),Cu(0.01)-ZnS	3.1015	5.3719	4.47	2.48	84
5	Ga(0.1),Cu(0.03)-ZnS	3.1015	5.3719	4.65	2.32	14
6	Ga(0.1),Cu(0.05)-ZnS	3.1015	5.3719	4.80	2.20	12

[a]The value was calculated from $2d_{111} \sin\theta = n\lambda$.
[b]The value was calculated from $a = d_{111}\sqrt{3}$.
[c]The value was calculated from Scherrer equation.
[d]The value was obtained from Tauc Plot.

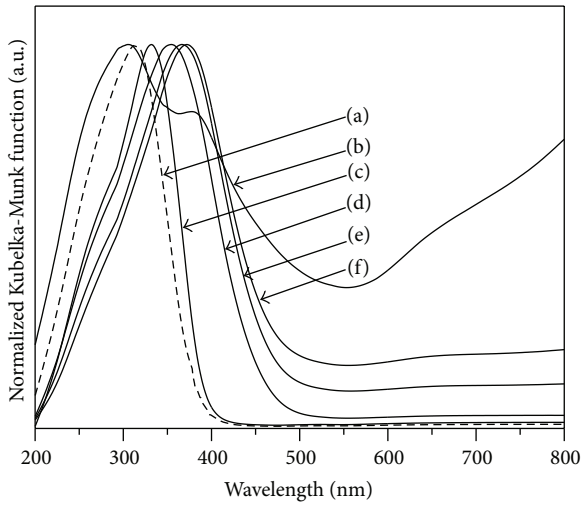

Figure 3: DR UV-visible spectra of (a) ZnS, (b) Cu(0.1)-ZnS, (c) Ga(0.1)-ZnS, (d) Ga(0.1),Cu(0.01)-ZnS, (e) Ga(0.1),Cu(0.03)-ZnS, and (f) Ga(0.1),Cu(0.05)-ZnS.

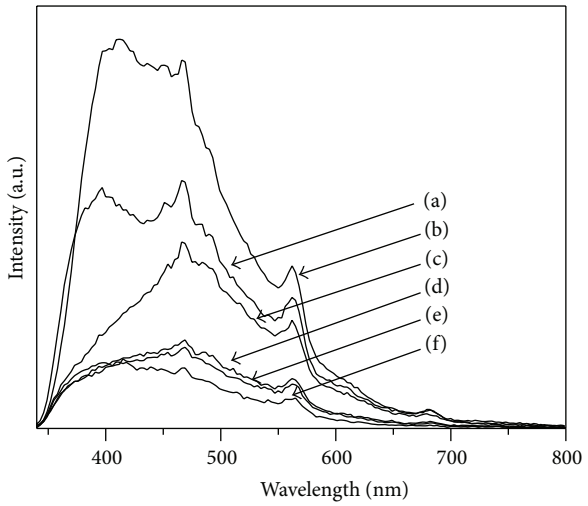

Figure 4: PL spectra of (a) ZnS, (b) Ga(0.1)-ZnS, (c) Ga(0.1), Cu(0.01)-ZnS, (d) Ga(0.1),Cu(0.03)-ZnS, (e) Ga(0.1),Cu(0.05)-ZnS, and (f) Cu(0.1)-ZnS.

Ga(0.1),Cu(x)-ZnS consists of donor levels of Cu 3d formed above the S 3p valence band. The band gap of Ga(0.1),Cu(x)-ZnS samples decreased with increasing Cu amount. Visible light absorption was only observed for samples doped with Cu. Therefore, the Cu metal ions play an important role in the absorption bands observed in the visible light region.

3.3.2. Photoluminescence Spectra. Figure 4 shows the comparison of photoluminescence (PL) spectra for all the samples in the range of 340 nm to 800 nm from the excitation wavelength of 250 nm. The intensity of the peak for ZnS and Ga(0.1)-ZnS is much stronger compared to the other samples, suggesting that these samples have high crystal quality with few defects. ZnS sample showed an absorption peak centered at 400 nm which might arise from electron-hole recombination. Three other broad peaks centered at 470 nm, 560 nm, and 690 nm were also observed. The broad peaks might be due to trap state emission arising from defect sites. The addition of dopant metal ions modifies the surface defect sites which in turn enhances or quenches the PL band. Although the emission spectra shape appeared similar, the decrease or increase in the PL intensity is evidence that the dopants enter into ZnS lattice. Only Ga(0.1)-ZnS showed higher intensity compared to ZnS.

The peak at 400 nm disappeared when Cu was doped in ZnS. This confirms that the peak around this region was due to electron-hole recombination emission of ZnS. No appreciable shifting of peak was noticed when Cu content increased. The peak intensity decreased with increasing Cu concentration. The decrease in intensity with increasing Cu content is due to repeated excitation within the copper dopant of the samples. Such a decrease in intensity with increasing copper loading was reported previously [34]. This was obvious for Cu(0.1)-ZnS where it has the lowest PL intensity.

3.4. Elemental Analysis. The surface chemical composition and chemical states of a representative sample, Ga(0.1), Cu(0.01)-ZnS, were analyzed by XPS as shown in Figure 5. The main peaks with binding energies associated with Zn (1025 eV, Zn $2p_{3/2}$ and 1048 eV, Zn $2p_{1/2}$), Ga (1149 eV, Ga

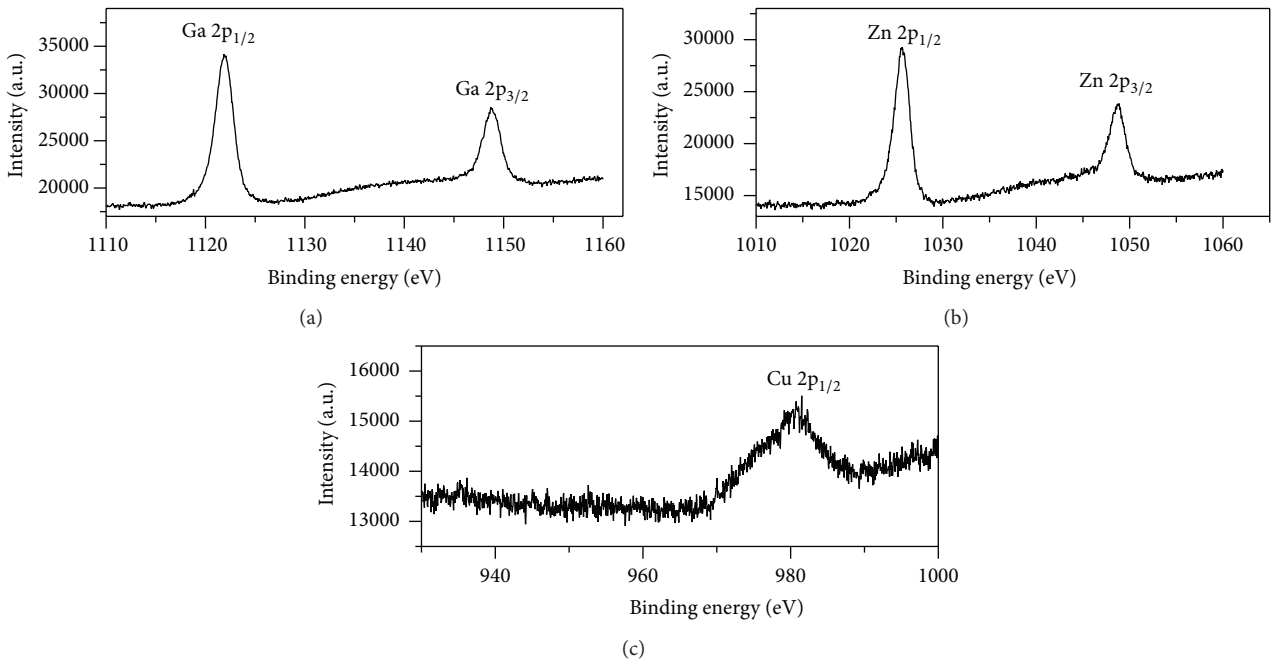

Figure 5: XPS spectra of Ga(0.1),Cu(0.01)-ZnS: (a) Ga, (b) Zn, and (c) Cu.

$2p_{3/2}$ and 1120 eV, Ga $2p_{1/2}$), Cu (981 eV, $2p_{1/2}$), S (165 eV, 2p), C (285 eV, 1s), and O (530 eV, 1s) were observed. The C and O peaks may originate from absorbed gaseous molecules and contamination caused by air exposure. The binding energies were also calibrated using carbon. There were no other element peaks indicating that the obtained product is relatively pure.

The binding energy corresponding to Ga $2p_{1/2}$ and $2p_{3/2}$ was found to shift towards higher values from the standard 1144 eV and 1117 eV to 1149 eV and 1120 eV, respectively. The shift of binding energy suggests some chemical interaction between the Ga^{3+} ions with other elements in the sample. A small peak corresponding to Ga $3d_{3/3}$ at 19 eV was also observed. The signal with binding energy of 20.9 eV is consistent with a trivalent Ga oxidation state [35]. The peaks of 1025.45 and 1048.85 eV can be attributed to Zn $2p_{3/2}$ and $2p_{1/2}$, respectively. This reveals the oxidation state of Zn^{2+} in the sample [36, 37]. The increase in the binding energy of Zn 2p bands may be seen as due to the interaction of Zn^{2+} ions with other elements on the surface. The measured binding energy of only Cu $2p_{1/2}$ was detected at 981.5 which was far from the value reported by other groups at around 950 [38]. This binding energy indicates that oxidation state of copper present was +2. Apart from being detected in a very small amount, Cu probably interacts with other metal ions present or forms new bond; thus the peak was largely shifted to higher energy. The single S2p peak at 165.75 eV was indicative of sulfur present as the divalent sulfur. The chemical compositions from XRF further support these findings.

The elemental contents of Ga, Cu, Zn, and S of all samples except ZnS were analyzed by XRF as listed in Table 2. The XRF data is similar to the added mol ratio during synthesis. The amount of Cu presence as detected by XRF increased with increasing amount of Cu during synthesis. From the elemental composition analysis, more Ga and Cu were detected on the surface (XPS) than in bulk (XRF) as compared to the representative sample Ga(0.1),Cu(0.01)-ZnS as shown in Table 3. This illustrates that both Ga and Cu are dispersed on the surface rather than present inside the bulk.

Table 2: Chemical composition of ZnS doped samples by XRF.

Entry	Samples	Zn	Cu	Ga	S
1	Cu(0.1)-ZnS	52.57	6.96	—	32.33
2	Ga(0.1)-ZnS	49.7	—	4.46	28.2
3	Ga(0.1),Cu(0.01)-ZnS	36.49	0.69	3.37	20.27
4	Ga(0.1),Cu(0.03)-ZnS	48.82	2.05	4.47	25.09
5	Ga(0.1),Cu(0.05)-ZnS	38.25	3.33	2.95	22.85

Table 3: Comparison of chemical composition from XRF and XPS.

Characterization method	Sample	Zn	Cu	Ga	S
XRF	Ga(0.1),Cu(0.01)-ZnS	36.49	0.69	3.37	20.27
XPS	Ga(0.1),Cu(0.01)-ZnS	37.30	7.90	46.59	8.21

3.5. Photocatalytic Activity. Figure 6 shows hydrogen evolution from an aqueous solution containing sacrificial reagents SO_3^{2-} and S_2^{2-} over Cu(0.1)-ZnS and Ga(0.1),Cu(x)-ZnS powder under visible light irradiation. Pure ZnS and Ga(0.1)-ZnS were not active to produce hydrogen under visible light irradiation due to their large band gap energy. The rate of hydrogen evolution over Cu(0.1)-ZnS was only 1.96 μmol/h. As Ga and Cu were codoped, the photocatalytic activity was greatly enhanced. The highest activity was observed for

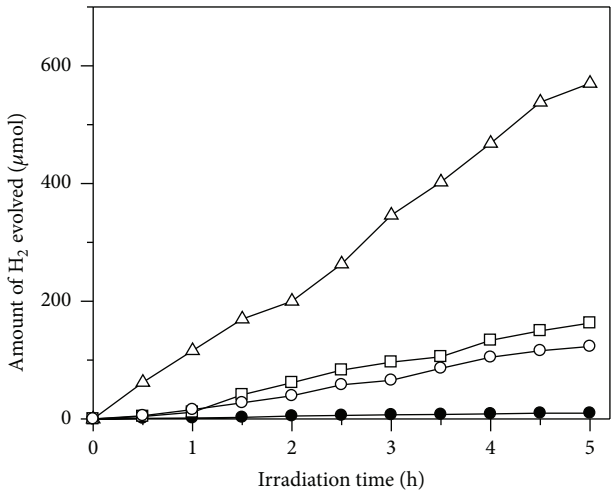

Figure 6: Photocatalytic hydrogen evolution on Cu(0.1)-ZnS (●), Ga(0.1),Cu(0.01)-ZnS (△), Ga(0.1),Cu(0.03)-ZnS (□), and Ga(0.1),Cu(0.05)-ZnS (○) under visible light irradiation.

Ga(0.1),Cu(0.01)-ZnS with the rate of hydrogen evolution reaching 114 μmol/h. Although the visible light absorption increased with increasing Cu content, the photocatalytic activity decreased. The high photocatalytic activity observed for Ga(0.1),Cu(0.01)-ZnS was dependent not only on the amount of Cu dopant but also on other factors. The presence of Ga was constant for each of the codoped samples. Small amount of Ga occupies the defect sites of ZnS [39]. It can be deduced that when optimum amount of Ga and Cu was used, they produce a synergistic effect that facilitates efficient charge carriers to participate in the photocatalytic activity. On the other hand, doping of a large amount of Cu ions would lead to charge recombination. Therefore, finding the optimum amount of dopants is crucial.

Another possible reason is that Ga(0.1),Cu(0.01)-ZnS possessed the smallest crystallite size as can be seen from the broad XRD peaks and largest surface area. Small crystallite size would facilitate fast transportation of photogenerated electrons from the bulk to surface avoiding their recombination in the bulk of the photocatalyst. On the other hand, enhancement in the surface area could afford more reaction sites. Both small crystallite size and large surface area are beneficial for enhanced photocatalytic activity. For this system, there should be a balance between the enhancement of visible light absorption and the increased electron-hole recombination. Therefore, decreased electron-hole recombination is desired for photocatalytic hydrogen process.

The stability of Ga(0.1),Cu(0.01)-ZnS was also examined for 15 hours as shown in Figure 7 without changing the sacrificial agent. For every 5 hours, the reaction system is degassed using nitrogen. The photocatalytic activity merely decreases at 5% after 15 hours. There was no sign of activity deterioration under the current photocatalytic reaction test in the presence of sacrificial reagents. It is important to note that there were no distinct changes in the physical properties after 15 hours of photoactivity measurements, indicating good stability of photocatalysts in the photocatalytic reaction.

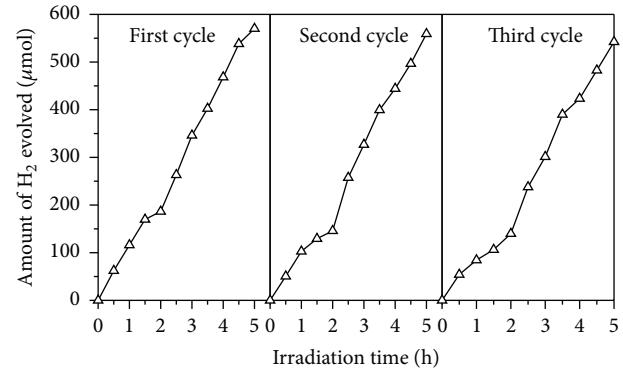

Figure 7: Stability test of Ga(0.1),Cu(0.01)-ZnS for 3 cycles under visible light irradiation.

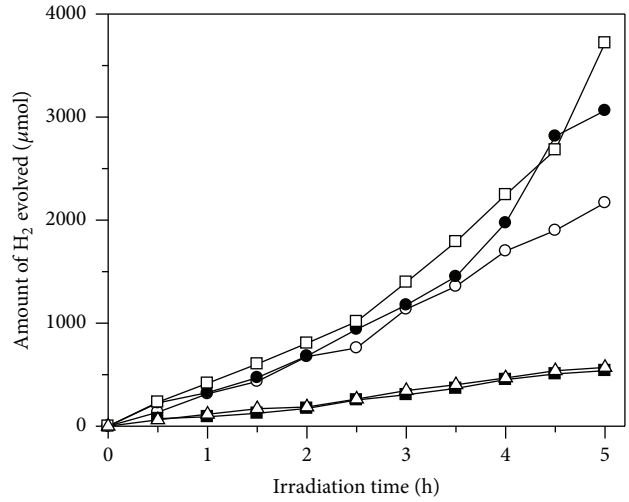

Figure 8: Photocatalytic hydrogen evolution on Ga(0.1),Cu(0.01)-ZnS (△), Ru(0.1 wt%)-Ga(0.1),Cu(0.01)-ZnS(○), Ru(0.3 wt%)-Ga(0.1),Cu(0.01)-ZnS (●), Ru(0.5 wt%)-Ga(0.1),Cu(0.01)-ZnS (□), and Ru(1 wt%)-Ga(0.1),Cu(0.01)-ZnS (■).

3.6. Cocatalyst. To improve further the photocatalytic activity, the effect of loading Ru as cocatalyst onto Ga(0.1),Cu(0.01)-ZnS was examined. Figure 8 shows the dependence of hydrogen evolution amount from an aqueous Na_2S and Na_2SO_3 solution over Ga(0.1),Cu(0.01)-ZnS on the loading amount of Ru cocatalyst. Before reaction, Ru (0.1, 0.3, 0.5, and 1 wt%) was deposited as a cocatalyst on photocatalysts by photodeposition method under visible light. Photocatalytic activity was markedly improved when the Ru cocatalyst was loaded on the Ga(0.1),Cu(0.01)-ZnS sample. It is well known that Ru has metallic characteristics with a higher conduction band potential above $2H^+/H_2$; hence reaction facilitates photoinduced electron/hole separation and thus inhibits their recombination effectively [40]. As shown in Figure 8, the hydrogen production rate increased with the increase of Ru content. When the Ru content increased to 0.5 wt%, the maximum activity for hydrogen production was attained. The average rate of hydrogen evolution amounts to 744 μmol/h, corresponding to an apparent quantum yield at

425 nm of 0.14%. Both below and above 0.5 wt% Ru content, the hydrogen evolution rate was lower. Ru as cocatalyst at optimum amount promoted the photogenerated charges separation and reduced recombination rate while acting as active sites for hydrogen production.

4. Conclusions

In summary, we have successfully synthesized Ga(0.1),Cu(x)-ZnS ($x = 0.01, 0.03, 0.05$) by hydrothermal method. These photocatalysts are active for photocatalytic hydrogen production under visible light irradiation. Ga was proposed as an effective dopant to introduce oxygen vacancies acting as efficient electron trap. The addition of Cu at optimum amount for Ga(0.1),Cu(0.01)-ZnS not only makes this photocatalyst active under visible light but also promotes the photocatalytic activity with hydrogen production rate of 114 μmol/h. Ru cocatalyst further improved the photocatalytic activity of Ga(0.1),Cu(0.01)-ZnS by 6.5 times. This works shows that Ga is an effective dopant for photocatalytic hydrogen production although Ga did not contribute to the visible light response of the photocatalyst. Codoping of two metal ions provided synergistic effect for the development of new photocatalyst for hydrogen production.

Conflict of Interests

The authors declare that there is no conflict of interests regarding the publication of this paper.

Acknowledgment

Financial support from the Ministry of Science, Technology and Innovation through the National Science Fellowship is greatly acknowledged (Melody Kimi).

References

[1] R. M. Navarro, M. C. Sánchez-Sánchez, M. C. Alvarez-Galvan, F. del Valle, and J. L. G. Fierro, "Hydrogen production from renewable sources: biomass and photocatalytic opportunities," *Energy & Environmental Science*, vol. 2, no. 1, pp. 35–54, 2009.

[2] R. M. Navarro Yerga, M. Consuelo Álvarez Galván, F. del Valle, J. A. Villoria de la Mano, and J. L. G. Fierro, "Water splitting on semiconductor catalysts under visiblelight irradiation," *ChemSusChem*, vol. 2, no. 6, pp. 471–485, 2009.

[3] P. V. Kamat, "Meeting the clean energy demand: nanostructure architectures for solar energy conversion," *Journal of Physical Chemistry C*, vol. 111, no. 7, pp. 2834–2860, 2007.

[4] J. Zhu and M. Zäch, "Nanostructured materials for photocatalytic hydrogen production," *Current Opinion in Colloid & Interface Science*, vol. 14, no. 4, pp. 260–269, 2009.

[5] K. Maeda and K. Domen, "New non-oxide photocatalysts designed for overall water splitting under visible light," *Journal of Physical Chemistry C*, vol. 111, no. 22, pp. 7851–7861, 2007.

[6] A. Kudo and Y. Miseki, "Heterogeneous photocatalyst materials for water splitting," *Chemical Society Reviews*, vol. 38, no. 1, pp. 253–278, 2009.

[7] J.-F. Reber and K. Meier, "Photochemical production of hydrogen with zinc sulfide suspensions," *Journal of Physical Chemistry*, vol. 88, no. 24, pp. 5903–5913, 1984.

[8] D. Hayes, F. Grieser, and D. N. Furlong, "Kinetics of hydrogen production from illuminated CdS/Pt/Na_2SO_3 and ZnS/Pt/Na_2S dispersions," *Journal of the Chemical Society, Faraday Transactions*, vol. 86, no. 21, pp. 3637–3640, 1990.

[9] S. K. Apte, S. N. Garaje, S. S. Arbuj et al., "A novel template free, one pot large scale synthesis of cubic zinc sulfide nanotriangles and its functionality as an efficient photocatalyst for hydrogen production and dye degradation," *Journal of Materials Chemistry*, vol. 21, no. 48, pp. 19241–19248, 2011.

[10] A. Kudo and M. Sekizawa, "Photocatalytic H_2 evolution under visible light irradiation on $Zn_{1-x}Cu_xS$ solid solution," *Catalysis Letters*, vol. 58, no. 4, pp. 241–243, 1999.

[11] T. Arai, S.-I. Senda, Y. Sato et al., "Cu-doped ZnS hollow particle with high activity for hydrogen generation from alkaline sulfide solution under visible light," *Chemistry of Materials*, vol. 20, no. 5, pp. 1997–2000, 2008.

[12] A. Kudo and M. Sekizawa, "Photocatalytic H_2 evolution under visible light irradiation on Ni-doped ZnS photocatalyst," *Chemical Communications*, no. 15, pp. 1371–1372, 2000.

[13] J. Zhang, S. Liu, J. Yu, and M. Jaroniec, "A simple cation exchange approach to Bi-doped ZnS hollow spheres with enhanced UV and visible-light photocatalytic H_2-production activity," *Journal of Materials Chemistry*, vol. 21, no. 38, pp. 14655–14662, 2011.

[14] R. Sasikala, V. Sudarsan, C. Sudakar, R. Naik, T. Sakuntala, and S. R. Bharadwaj, "Enhanced photocatalytic hydrogen evolution over nanometer sized Sn and Eu doped titanium oxide," *International Journal of Hydrogen Energy*, vol. 33, no. 19, pp. 4966–4973, 2008.

[15] R. Jaiswal, N. Patel, D. C. Kothari, and A. Miotello, "Improved visible light photocatalytic activity of TiO_2 co-doped with Vanadium and Nitrogen," *Applied Catalysis B: Environmental*, vol. 126, pp. 47–54, 2012.

[16] M.-Y. Lu, M.-P. Lu, Y.-A. Chung, M.-J. Chen, Z. L. Wang, and L.-J. Chen, "Intercrossed sheet-like Ga-doped ZnS nanostructures with superb photocatalytic actvitiy and photoresponse," *The Journal of Physical Chemistry C*, vol. 113, no. 29, pp. 12878–12882, 2009.

[17] N. Arai, N. Saito, H. Nishiyama, Y. Inoue, K. Domen, and K. Sato, "Overall water splitting by RuO 2-dispersed divalent-ion-doped GaN photocatalysts with d 10 electronic configuration," *Chemistry Letters*, vol. 35, no. 7, pp. 796–797, 2006.

[18] N. Arai, N. Saito, H. Nishiyama et al., "Effects of divalent metal ion (Mg^{2+}, Zn^{2+} and Be^{2+}) doping on photocatalytic activity of ruthenium oxide-loaded gallium nitride for water splitting," *Catalysis Today*, vol. 129, no. 3-4, pp. 407–413, 2007.

[19] Y. C. Chen, C. H. Wang, W. T. Chen, B. H. Li, L. W. Tub, and C. P. Liu, "Undoped and Ga-doped hexagonal platelet interconnected ZnS nanowires: cathodoluminescence and metal—semiconductor electron transport transition," *Scripta Materialia*, vol. 64, no. 8, pp. 761–764, 2011.

[20] X. Zhang, D. Jing, M. Liu, and L. Guo, "Efficient photocatalytic H_2 production under visible light irradiation over Ni doped $Cd_{1-x}Zn_xS$ microsphere photocatalysts," *Catalysis Communications*, vol. 9, no. 8, pp. 1720–1724, 2008.

[21] M. Kimi, L. Yuliati, and M. Shamsuddin, "Photocatalytic hydrogen production under visible light over $Cd_{0.1}Sn_xZn_{0.9-2x}S$ solid solution photocatalysts," *International Journal of Hydrogen Energy*, vol. 36, no. 16, pp. 9453–9461, 2011.

[22] S. Zu, Z. Wang, B. Liu, X. Fan, and G. Qian, "Synthesis of nano-$Cd_xZn_{1-x}S$ by precipitate-hydrothermal method and its

photocatalytic activities," *Journal of Alloys and Compounds*, vol. 476, no. 1-2, pp. 689–692, 2009.

[23] S. Sain and S. K. Pradhan, "Mechanochemical solid state synthesis of $(Cd_{0.8}Zn_{0.2})S$ quantum dots: Microstructure and optical characterizations," *Journal of Alloys and Compounds*, vol. 509, no. 10, pp. 4176–4184, 2011.

[24] Y. Zhao, Y. Zhang, H. Zhu, G. C. Hadjipanayis, and J. Q. Xiao, "Low-temperature synthesis of hexagonal (wurtzite) ZnS nanocrystals," *Journal of the American Chemical Society*, vol. 126, no. 22, pp. 6874–6875, 2004.

[25] M. Saranya, R. Ramachandran, E. J. J. Samuel, S. K. Jeong, and A. N. Grace, "Enhanced visible light photocatalytic reduction of organic pollutant and electrochemical properties of CuS catalyst," *Powder Technology*, vol. 279, pp. 209–220, 2015.

[26] M. Saranya, C. Santhosh, R. Ramachandran et al., "Hydrothermal growth of CuS nanostructures and its photocatalytic properties," *Powder Technology*, vol. 252, pp. 25–32, 2014.

[27] U. T. D. Thuy, N. Q. Liem, C. M. A. Parlett, G. M. Lalev, and K. Wilson, "Synthesis of CuS and CuS/ZnS core/shell nanocrystals for photocatalytic degradation of dyes under visible light," *Catalysis Communications*, vol. 44, pp. 62–67, 2014.

[28] G. Zhang, X. Zou, J. Gong et al., "Characterization and photocatalytic activity of Cu-doped $K_2Nb_4O_{11}$," *Journal of Molecular Catalysis A: Chemical*, vol. 255, no. 1-2, pp. 109–116, 2006.

[29] B. Liu, L. Hu, C. Tang et al., "Self-assembled highly symmetrical ZnS nanostructures and their cathodoluminescence," *Journal of Luminescence*, vol. 131, no. 5, pp. 1095–1099, 2011.

[30] O. Kozák, P. Praus, K. Kočí, and M. Klementová, "Preparation and characterization of ZnS nanoparticles deposited on montmorillonite," *Journal of Colloid and Interface Science*, vol. 352, no. 2, pp. 244–251, 2010.

[31] G. R. Chaudhary, P. Bansal, and S. K. Mehta, "Recyclable CuS quantum dots as heterogeneous catalyst for Biginelli reaction under solvent free conditions," *Chemical Engineering Journal*, vol. 243, pp. 217–224, 2014.

[32] X. Qiu, M. Miyauchi, H. Yu, H. Irie, and K. Hashimoto, "Visible-light-driven Cu(II)–$(Sr_{1-y}Na_y)(Ti_{1-x}Mo_x)O_3$ photocatalysts based on conduction band control and surface ion modification," *Journal of the American Chemical Society*, vol. 132, no. 43, pp. 15259–15267, 2010.

[33] A. Datta, S. K. Panda, and S. Chaudhuri, "Phase transformation and optical properties of Cu-doped ZnS nanorods," *Journal of Solid State Chemistry*, vol. 181, no. 9, pp. 2332–2337, 2008.

[34] M. Wang, L. Sun, X. Fu, C. Liao, and C. Yan, "Synthesis and optical properties of ZnS:Cu(II) nanoparticles," *Solid State Communications*, vol. 115, no. 9, pp. 493–496, 2000.

[35] A. S. Deshpande, D. G. Shckukin, E. Ustinovicetti, M. Antoni, and R. A. Carusoh, "Titania and mixed titania/aluminum, gallium, or indium oxide spheres: sol-gel/template synthesis and photocatalytic properties," *Advanced Functional Materials*, vol. 15, no. 2, pp. 239–245, 2005.

[36] Y.-N. NuLi, Y.-Q. Chu, and Q.-Z. Qin, "Nanocrystalline $ZnFe_2O_4$ and Ag-doped $ZnFe_2O_4$ films used as new anode materials for Li-ion batteries," *Journal of the Electrochemical Society*, vol. 151, no. 7, pp. A1077–A1083, 2004.

[37] Y. Sharma, N. Sharma, G. V. S. Rao, and B. V. R. Chowdari, "Li-storage and cyclability of urea combustion derived $ZnFe_2O_4$ as anode for Li-ion batteries," *Electrochimica Acta*, vol. 53, no. 5, pp. 2380–2385, 2008.

[38] I. H. Tseng, J. C. S. Wu, and H. Y. Chou, "Effects of sol–gel procedures on the photocatalysis of Cu/TiO_2 in CO_2 photoreduction," *Journal of Catalysis*, vol. 221, no. 2, pp. 432–440, 2004.

[39] A. Ali, X. Zhao, A. Ali et al., "Enhanced photocatalytic activity of ZnO nanorods grown on Ga doped seed layer," *Superlattices and Microstructures*, vol. 83, pp. 422–430, 2015.

[40] J.-Y. Liu, B. Garg, and Y.-C. Ling, "$Cu_xAg_yIn_zZn_kS_m$ solid solutions customized with RuO_2 or $Rh_{1.32}Cr_{0.66}O_3$ co-catalyst display visible light-driven catalytic activity for CO_2 reduction to CH_3OH," *Green Chemistry*, vol. 13, no. 8, pp. 2029–2031, 2011.